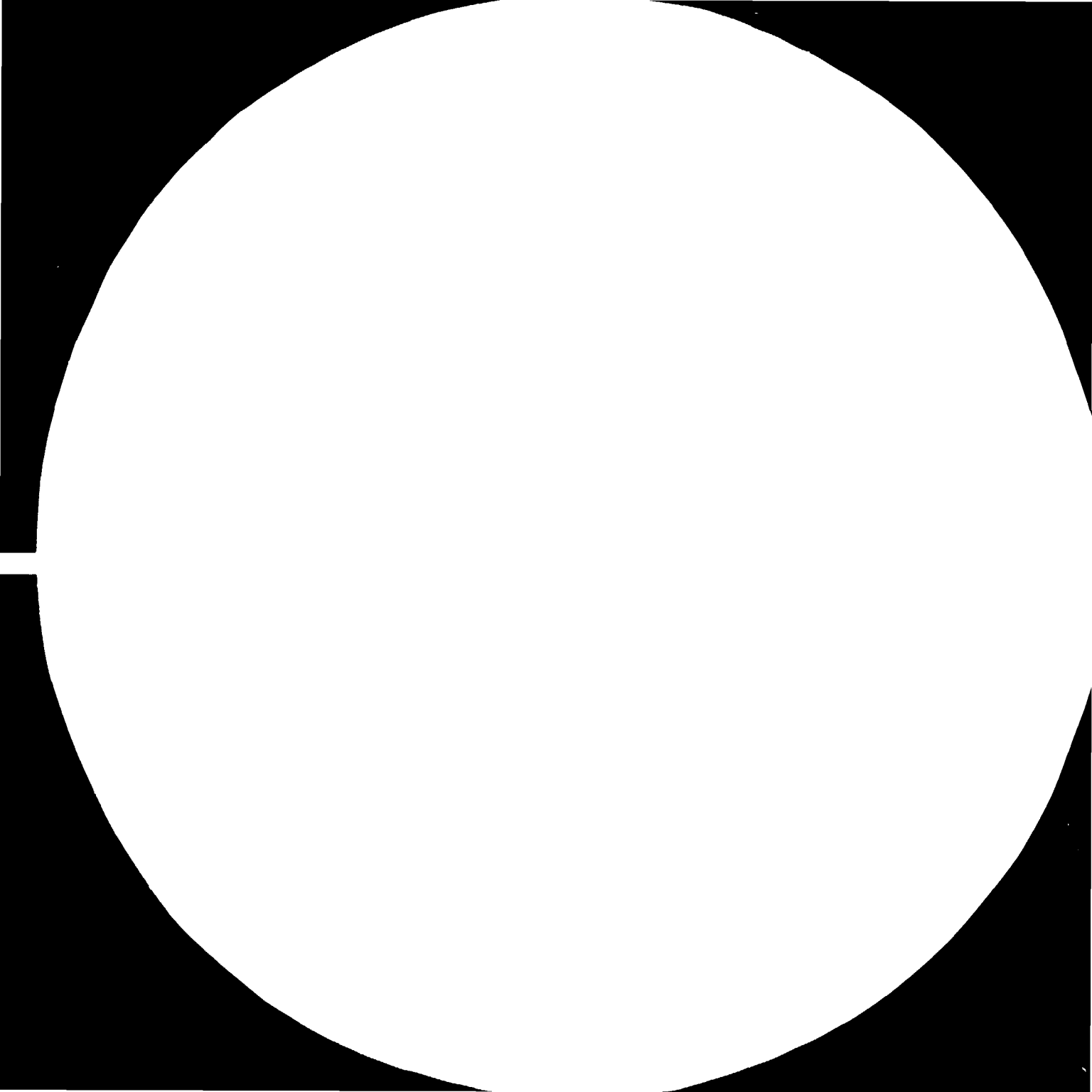

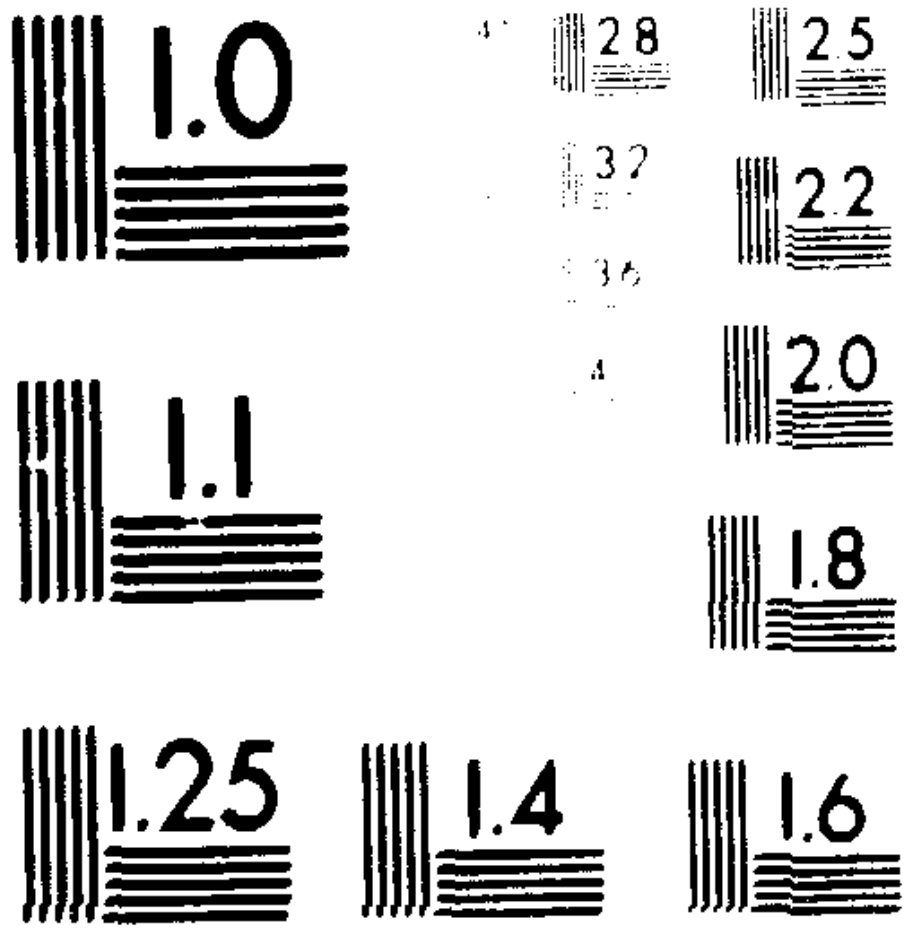

NIKHEF

NATIONAAL INSTITUUT VOOR KERNFYSICA EN HOGE-ENERGIEFYSICA

June 1986

NIKHEF-H/86-12

A DRIFT CHAMBER WITH VARIABLE DRIFT VELOCITY

F. Hartjes, J. Timmermans, F. Udo and N. Zonjee,

NIKHEF-H, Amsterdam, The Netherlands

ABSTRACT:

A wedge type drift chamber is planned to be used as part of the inner detector of the DELPHI-experiment. The chamber features drift velocities (carefully controlled) proportional to the total drift distance to facilitate triggering. The gas choice and its consequences for calibration with and without magnetic field are discussed.

Long-term stability and the effect of a magnetic field have been measured with a prototype drift chamber. Most tests reported here have been done with a laser beam with single wire accuracies below 20 micron.

Submitted to Nuclear Instr. and Methods in Physics Research

1. INTRODUCTION

High-energy colliding beam experiments generally measure the pattern of the particles emerging from the collision region enclosed by the beampipe with a small gas chamber. Thereafter, momentum, velocity and calorimetric measurements complete the information about the stable particles produced in the reaction. Physics dictates, that the detectors cover as large a solid angle as possible around the collision region (4π geometry).

A cylindrical multiwire chamber has been chosen by the DELPHI group as first detector around the beampipe[1]. The design has two parts: a jet type chamber to measure accurately the trajectory of the outgoing particles in the plane perpendicular to the primary beams and five layers of proportional chambers which measure the coordinate along the beam direction via cathode strip read-out.

Figures 1 & 2 show the cross sections of the detector in the two projections. The inner part consists of 24 drift cells extending from a radius of 123 mm to 220 mm. Consequently the maximum drift path varies from 16 mm to 29 mm.

The detector will operate in a magnetic field of 1.2 Tesla parallel to the wires and perpendicular to the drift direction, hence the Lorentz angle became an important concern in the design. It should preferably be kept small and constant throughout the chamber.

Another requirement for the design was to produce a fast track trigger which selects tracks coming from the interaction region. The jet design allows to do this via a simple coincidence, if for good tracks the anode pulses are coincident or nearly so. The drift distances increase with radius, so this trigger concept requires drift velocities increasing with radius to arrive at equal drift times for good tracks.

Section 2 describes how the drift properties of CO_2 are perfect to fulfil

these requirements. The question remained if such a counter with different electron drift speeds is practical as a real detector. The prototype work described in Section 3 & 4 gives an affirmative answer to these questions.

2. THE DRIFT GAS

In simple transport theory[2] the relation between the Lorentz angle α_L, the drift velocity at zero magnetic field v_0, the drift field E and the magnetic field B can be written as:

$$\tan \alpha_L = v_0 \cdot B/E \qquad (1)$$

The variation of the drift velocity due to B is given by:

$$v_0 = v_B \cdot \sqrt{1 + \tan^2 \alpha_L} \qquad (2)$$

It follows, that α_L and v_0/v_B are independent of the drift field as long as v_0 is proportional to E. CO_2 is a drift gas having just this property below drift fields of about 2 KV/cm. Moreover it has a diffusion coefficient which is near to the thermal limit.

Our measurements of the drift velocity and the diffusion constant of a mixture of 95% CO_2 and 5% isobutane at NTP are presented in table 1 and shown in figures 3 & 4. The results are obtained by using single-electron events generated by a beam of light from a two-step nitrogen laser in a program to measure the parameters of several drift chamber gasses.

The measurements are in agreement with earlier results[3], but with increased range and accuracy. The drift velocity curve shows a slight deviation from linearity above 1.5 KV/cm which is important to include in the calculation of the performance of the chamber. From these data one calculates in agreement with Becker et al.[3] that $\alpha_L \approx 5°$ at 1.0 Tesla in CO_2, thus $v_0/v_B = 1.004$ as long as the drift velocity is proportional to E. The diffusion data tells us, that CO_2 works best as a drift gas with electric fields above 1 KV/cm.

The geometry as shown in figure 1 ensures, that only tracks coming from the origin have drift distances proportional to the radius r. If the drift velocity is proportional to r we obtain coincident anode pulses for good, straight tracks. The chosen drift velocities vary between 10 and 20 micron per nsec, so a time window of 100 nsec determines the position and straightness of a track to better than one to two millimeters. Bending and displacement of tracks can be neglected in the 10 cm of track segment seen by the jet chamber provided the transverse momentum is more than 1.5 GeV/c.

3. CALIBRATION AND STABILITY TESTS

A full-size prototype of one sector was built. Figure 5 shows a cross section. This prototype was constructed with a drift volume accepting ±11.5° from the detector plane instead of ±7.5° in the final design. This ensures that edge effects from the rather coarse field cage are negligible.

Figure 6 illustrates the electrostatic configurations of the prototype and of the final cell to be used. It is clear, that the electron paths will not be perpendicular to the anode plane and will be slightly curved because the electric field increases with radius. The drift fields are 1.3 KV/cm at a radius of 123 mm and 2.5 KV/cm at the outer radius of 220 mm. The prototype shows edge effects due to the coarse strip structure of the cathodes, but this effect is negligible below angles of 10° with respect to the anode plane. Most measurements are done in an interval of ±8° where the two fields are nearly identical.

Figure 7 shows the prototype wedge chamber plus the laser set-up. The laser was a two-stage nitrogen laser[5] emitting a nearly diffraction limited beam. The beam was sent into the chamber via a pentaprism mirror C and a rotateable mirror D. The position of D was recorded via a shaft encoder with a resolution of 63 microradian. Rotating D could simulate tracks coming from -11.5° to +11.5°

through the chamber. The track origin could be centered or off-centered by moving the system C and D on a common support.

The beam width adapter (A_1,A_2) focussed the beam at the end of the chamber. The focal length was 70 cm. The reference diode was used to trigger the recording system but also to monitor the intensity of the beam. Only laser pulses deviating no more than 15% from the nominal intensity were accepted. The laser ran at 3 Hz and a typical run took only a couple of minutes to obtain 200 accepted pulses. The ionization of the laser in the chamber was enhanced by adding some dimethyl aniline to the gas. The averages per wire over 200 measurements were used in a straight line fit over the 24 points. Typical deviations from this fit were between 6 and 20 microns per wire. These values were mainly determined by the spatial beam stability in the second stage of the laser.

The chamber gas was 95% CO_2 and 5% isobutane. Its composition was controlled by two mass flow controllers. The oxygen content was monitored and kept between 30 and 50 ppm. This is high for drifting electrons in CO_2 but the relatively high drift fields used limited the absorption of electrons to maximally 20%. The temperature and pressure were recorded at every run as the drift speed is proportional to T/P.

The 24 anode signals were processed by a standard preamplifier-discriminator system sending its pulses to 24 channels of LeCroy 4208 TDC. A straight track coming from the origin should produce 24 coincident signals. Figure 8 shows these patterns from the prototype. It is clear, that the principle works and that the prototype field cage was not perfect. The points at large drift times show the response to a track which has the same direction but is displaced by 3 mm at the origin (mirror D).

The counter was calibrated by measuring the laser tracks at both sides of

the anode plane in 1° intervals and storing the drifttimes of each wire as a reference. The result was that the behaviour of the drifting electrons can be characterized by an angular velocity of about $6 \cdot 10^{-3}$ degree per nsec plus a small quadratic term.

After writing such a file we remeasured daily one angular setting during one month without touching the apparatus. The drift times were corrected for temperature and pressure variations. For every run an angle and extrapolated zero position were calculated with the help of the calibration file. Both the measured angle and the extrapolated zero showed a big dispersion from run to run, far too much to be tolerable for an accurate track measurement. Figure 9 shows, though, that there exists a correlation between measured angle and origin of the laser beam. In fact this correlation is in agreement with the constants of the optical system: the laser beam was wandering through the aperture of the optical system. The dashed line represents the correlation as given by the diaphragm and lenses A_1 and A_2.

We observe that the deviation of the points from the line is less than 20 micron, thus we conclude that the stability of the counter is better than 20 micron over a period of one month during which the pressure did vary between 1006 and 1020 mbar and the temperature between 13 and 20 °C.

This calibration has been used in a test with cosmics. The geometry was such that 30 cm of the anode wires was used and the crossing angles were between +45° and -45° with the wire direction. Furthermore only the tracks within the volume of ±7.5° from the anode plane were accepted.

Fitting these tracks to a straight line gave fits with an average RMS of 78 microns per wire for all tracks. This number includes all errors one usually has in a real experiment except background effects. Tracks crossing the anode plane were used to tune the two halves of the detector. The result was 110 microns per

point, for crossing tracks having minimally 12 points in the calibrated drift regions.

One year after these runs the prototype was tested at CERN with laser tracks. The by then one year old calibration file still produced a straight line fit of 42 micron per wire. The absolute position could not be checked as the apparatus had been dismantled and rebuilt with different mechanical components.

4. MEASUREMENTS IN A MAGNETIC FIELD

The aims of this test, performed with essentially the same apparatus, were to show that:

(a) the chamber operates correctly in a magnetic field,

(b) the Lorentz angle is constant for the different drift fields used in the drift volume,

(c) the drift velocity is nearly unaffected by the magnetic field,

(d) one can derive the calibration in a magnetic field from data taken without field.

The field of .95 Tesla was provided by a magnet having interior dimensions of $0.8 \times 1.24 \times 2.0$ m^3. The field lines were horizontal and 1.24 m long. The prototype was set up with its wires parallel to the magnetic field. A major problem was that the magnet, when switched on, moved by about 0.4 mm with respect to the laser.

The laser beam was used in two different modes:

Parallel beam

This is a narrow beam of about 0.4 mm diameter capable of producing a continuous ionization. The set-up was essentially the same as depicted in figure 7.

Focussed beam

Here the beam was first widened to 1 cm diameter and then focussed by a lens with low spherical aberrations (f=20 cm) into a point in the chamber. The focal point could be positioned remotely by shifting the position of this lens along the beam. Sixty percent of the ionization was found to be concentrated within 0.8 mm in the beam direction. Transverse dimensions were in the order of 20 microns in this case.

The answer to the first point stated above was unambiguous: apart from a slight shift in drift times no difference could be detected in pulse height or RMS per point between operation without or with .95 Tesla field.

4.1. The Lorentz angle was measured by scanning the focus of the laser beam through the drift volume in steps of 1 mm in the beam direction at several angles to the anode plane. The anode wires are numbered one to twenty-four, going from small to large distances from D. Wires 7 to 16 were now also connected to an ADC.

The results of a scan for amplitude are illustrated in figure 10. Experience had shown, that the separation between cells as defined by the crossing of the amplitudes in fig. 10 gave the best definition of the cell position in space. This implied that in this case we worked relative to the position of the grid wires, so the effective drift paths used in the calculation of drift angles were taken 2 mm shorter than the nominal value. This had the added advantage of excluding a region in the chamber, where the electric field was very rapidly varying. Figure 11 gives

the positions of the acceptances of the cells as defined from data as presented in figure 10. One sees clearly the asymmetric effect of the magnetic field.

Ideally the electric field should be normal to the anode wire plane, but the field has to increase linearly with radius. The effect of this condition is to introduce a small perpendicular component, compelling the electrons to follow a path which is inclined at about 5° to the anode wire plane. The equipotential lines in figure 6 show this effect.

The drift paths without magnetic field are nearly straight. Electrostatic calculations show that the zero field angles and the Lorentz angle at 1 Tesla nearly compensate at one side of the wire plane. This means that the dotted curves in figure 11 at negative angles follow the relation $r(\Theta)=r/\cos\Theta$.

From the data presented in figure 11 one can calculate the Lorentz angles. The data showed no systematic variation, so the second statement from the introduction is confirmed. The average Lorentz angle is:

$\alpha_L = 4.92° \pm 0.08°$, at 0.95 Tesla.

The error was calculated from the RMS of all results together.

Formula (1) predicts α_L to be three percent higher at drift fields around 2 KV/cm. This effect has not been seen in the data.

4.2. Drift velocity and time-angle relations

Without magnetic field the calibration of the chamber was simple: one generated straight tracks through the chamber volume with a laser beam coming from the origin. The adjustment of the origin was done by measuring symmetrically around the origin and repeatedly adjusting the orientation and position of the chamber. A comparison between field on and off was complicated by the movement of the magnet under power which moved both the origin and the zero angle of the beam.

It was impossible to readjust the chamber again with field on. An added

complication was that with current on the temperature in the magnet was slowly rising by about 1 °C per hour. This created an uncertainty about the temperature inside the counter of this order, thus an error in the drift velocity of 3×10^{-3}. Consequently the runs with magnet on and off had to be alternated, hence it was impossible to rely on the laser beam as an absolute reference.

We tried to minimize the influence of the mechanical instabilities of the set-up by deriving angular drift speeds from the time-angle relations as these drift speeds are to first order constant in the whole drift space, so that small position and angular errors do not matter. We parametrized the time-angle relations for every wire by:

$$t_i = a_i\theta^2 + b_i\theta + c_i, \qquad (i = 1 \text{ to } 24)$$

and fitted this formula to the measured drift times t_i for angles between 1° and 7.5°.

In principle c_i represents the off-sets which we discard and so we only look at the slopes of the time-angle relation:

$$dt/d\theta = 2a_i\theta + b_i.$$

Six of these time-angle relations were measured: left and right of the anode plane for B=0, +0.95 Tesla and -0.95 Tesla.

Table 2 presents the actual angular drift velocities at 5° for the three field situations measured at wire 8, 12 and 16. The positive and negative field measurements are each compared with the no-field calibrations on the same day so as to eliminate as much as possible the temperature uncertainties. From these data one calculates v_0/v_B. The result is given in the last column of table 2.

The average for positive angles is: $v_0/v_B = 1.0044$,

The average for negative angles is: $v_0/v_B = 1.0074$.

It is clear from table 2 that although we tried to eliminate the effects of temperature and asymmetries, we did not succeed completely. However, the change

in the drift velocity due to the magnetic field is certainly small and close to the value of 1.004 calculated from elementary transport theory.

Table 3 shows the differences in drift speed as derived from table 2. It is clear that in case the magnetic and electric drift angles compensate one can apply a correction of -0.3% to the field-free data to obtain the calibration with field: the drift times become slightly shorter.

The opposite case gives +2.6% and +2.0% correction for the two halves of the detector. This is clearly an asymmetry which did not occur in the Lorentz angle determination and we attribute it to temperature drifts during the measurements.

Tables 2 and 3 can be regarded as part of the calibration files without and with field. Are the corrections due to the magnetic field measured well enough to be used on a field-free calibration?

The electrostatic calculations were able to reproduce the total drift times of the prototype to a few percent, and gave -0.6% and +2.4% for the correction due to the field. The measurements as shown here confirm these results, so we assume, that the effects of the magnetic field on the final detector can be calculated to an accuracy with systematic errors of no more than 2‰ or 20 to 40 microns in the time-angle relation calibration.

Acknowledgement

We thank our DELPHI colleagues for many fruitful discussions and the technical staff of the NIKHEF-laboratory for the accurate construction of the test chamber and laser set-up.

REFERENCES

[1] DELPHI Technical Proposal, CERN/LEPC 83-3.

[2] V. Palladino and B. Sadoulet, Nucl. Instr. Meth. 128 (1975) 323.

[3] Drift velocities:

U. Becker et al., Nucl. Instr. Meth. 214 (1983) 525.

Diffusion:

G. Schultz, Thesis Strasbourg 1976,
CERN EP 76-19.

J.P. Fehlmann et al., ETH Zuerich, 1983.

[4] Fabricated by TNO Kunststoffen Instituut, Delft, Holland.
The compression test has been done over a period of one year. No creap was detected.

[5] J. Konijn en F. Hartjes, Nucl. Instr. Meth. 217 (1983) 311.

TABLE 1

Drift velocity v_0 and longitudinal diffusion coefficient D_L of CO_2/iso C_4H_{10} 95/5 at 20 °C and 1000 mbar pressure.

The errors given are statistical. The velocity measurements might contain a scale error of about 1%.

Drift field E	v_D	D_L
(KV/cm)	micron/nsec	microns/ cm
.30	2.299 ± 0.004	136 ± 3
.40	3.011 ± .003	114 ± 3
.50	3.731 ± .003	101 ± 2
.60	4.450 ± .003	101 ± 3
.70	5.177 ± .003	96 ± 2
.80	5.905 ± .004	83 ± 3
.90	6.663 ± .004	90 ± 5
1.00	7.436 ± .004	80 ± 3
1.10	8.209 ± .005	87 ± 4
1.20	9.004 ± .005	83 ± 3
1.30	9.791 ± .004	88 ± 3
1.40	10.602 ± .004	78 ± 2
1.50	11.420 ± .005	84 ± 3
1.60	12.283 ± .005	83 ± 2
1.70	13.143 ± .006	81 ± 3

1.80	14.047 ± .006	79 ± 3
1.90	14.989 ± .008	81 ± 5
2.00	15.888 ± .009	83 ± 3
2.10	16.838 ± .009	78 ± 5
2.20	17.872 ± .011	78 ± 4
2.30	18.839 ± .011	74 ± 6
2.40	19.913 ± .013	63 ± 12
2.50	21.028 ± .015	77 ± 12
2.60	22.141 ± .017	-
2.70	23.324 ± .019	-
2.80	24.581 ± .022	-

• • •

TABLE 2.

Angular velocities in nsec / degree

		-9.5 KG	-Zero	-9.5 KG	-Zero	V_0/v_B
Wire #8	-5°	154.7	155.2	158.9	156.0	1.0037
	-5°	163.5	159.3	160.8	161.1	1.0082
Wire #12	-5°	149.5	149.8	153.8	150.9	1.0043
	-5°	156.9	152.8	153.9	154.4	1.0064
Wire #16	-5°	145.9	146.4	151.2	147.9	1.0052
	-5°	152.9	148.6	149.4	150.1	1.0077
Thus	-5°	v_0/v_B	1.0044			
on average	-5	v_0/v_B	1.0074			

TABLE 3.

Differences in drift speed in nsec per degree due to the magnetic field.

		(-0.95 T)-Zero	(-0.95 T)-Zero
Wire #8	-5	-0.5 (-0.3%)	2.9 (1.8%)
	-5°	4.2 (2.6%)	-0.3 (-0.2%)
Wire #12	-5°	0.3 (-0.2%)	2.9 (1.9%)
	5°	4.1 (2.6%)	-0.5 (-0.3%)
Wire #16	-5	0.5 (-0.3%)	3.3 (2.2%)
	5°	4.3 (2.8%)	-0.7 (-0.5%)

FIGURE CAPTIONS

(1) Cross section of the inner detector of the DELPHI experiment perpendicular to the beam. All wires are parallel to the beam axis.

The inner part is a jet type drift chamber with 24 sectors, the outer part is formed by 5 proportional chambers with cathode read-out.

Some mechanical details are:

* walls / composite epoxy/aramide cylinders of 1.3 mm thick,
* compression under a load of 10000 N: 300 micron[4)],
* anode wire plane / 24 wires - 20 micron W/Au,
* grid plus cathode planes / 48 wires - 50/70 micron Cu/Be.

(2) Cross section of the inner detector parallel to the beam.

(3) Drift velocity v_D versus drift field E_D in CO_2 at normal temperature and pressure.

The measurement error is smaller than the size of the points.

(4) Longitudinal diffusion coefficient D_L of CO_2, as a function of drift field.

(5) Prototype of one drift cell.

The acceptance of the drift section is larger than in the final detector ($\pm 11.5°$ versus $\pm 7.5°$).

(6) Electrostatic equipotential lines in one drift cell for the prototype (a) and

the final cell (b).

The drift field is varying from 1.2 KV/cm to 2.3 KV/cm going from a radius of 123 mm to 220 mm. The anode-grid voltage difference is +2.3 KV.

(7) Test set-up with laser installation.

(8) Drift time versus anode wire number for tracks at 5°. The points without fit are obtained by displacing the track parallel over 3 mm.

It is clear that a coincidence condition with a window of 100 nsec will distinguish between the two tracks.

(9) Relation between track angle and extrapolated origin for tracks measured during one month at 3.5°.

(10) Amplitude scan through the drift chamber along a track at 4°. The upper trace is the total charge from the chamber, the dotted lines the response of the individual anode wires.

(11) Result of the amplitude scans for zero field (continuous lines) and 0.95 Tesla field.

The dotted lines at negative angles follow closely the relation:

$r = r_i(\cos\theta)^{-1}$, thus they represent drift paths perpendicular to the anode plane.

* * *

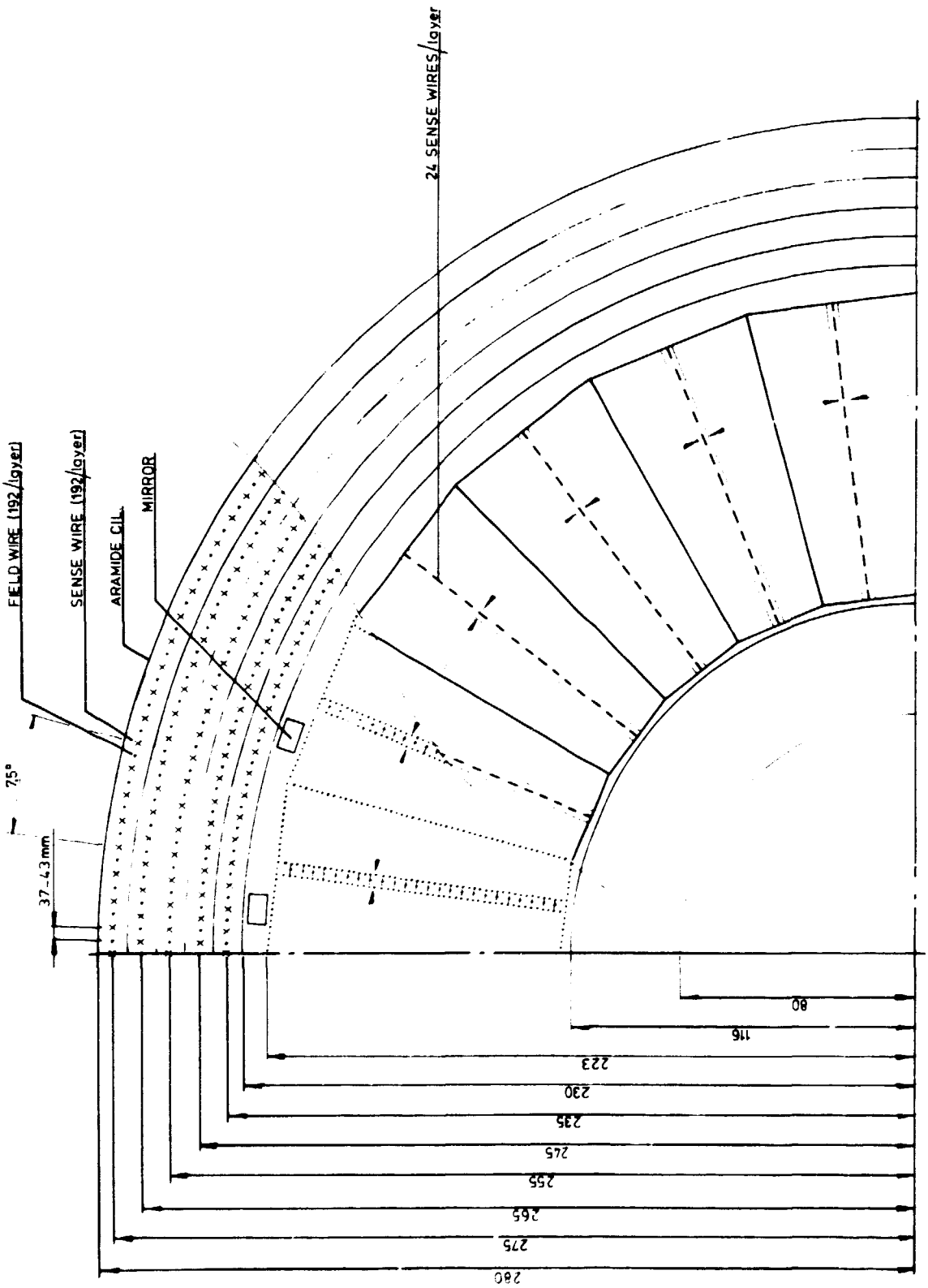

Fig. 1 LAY OUT INNER DETECTOR (revised Feb85)

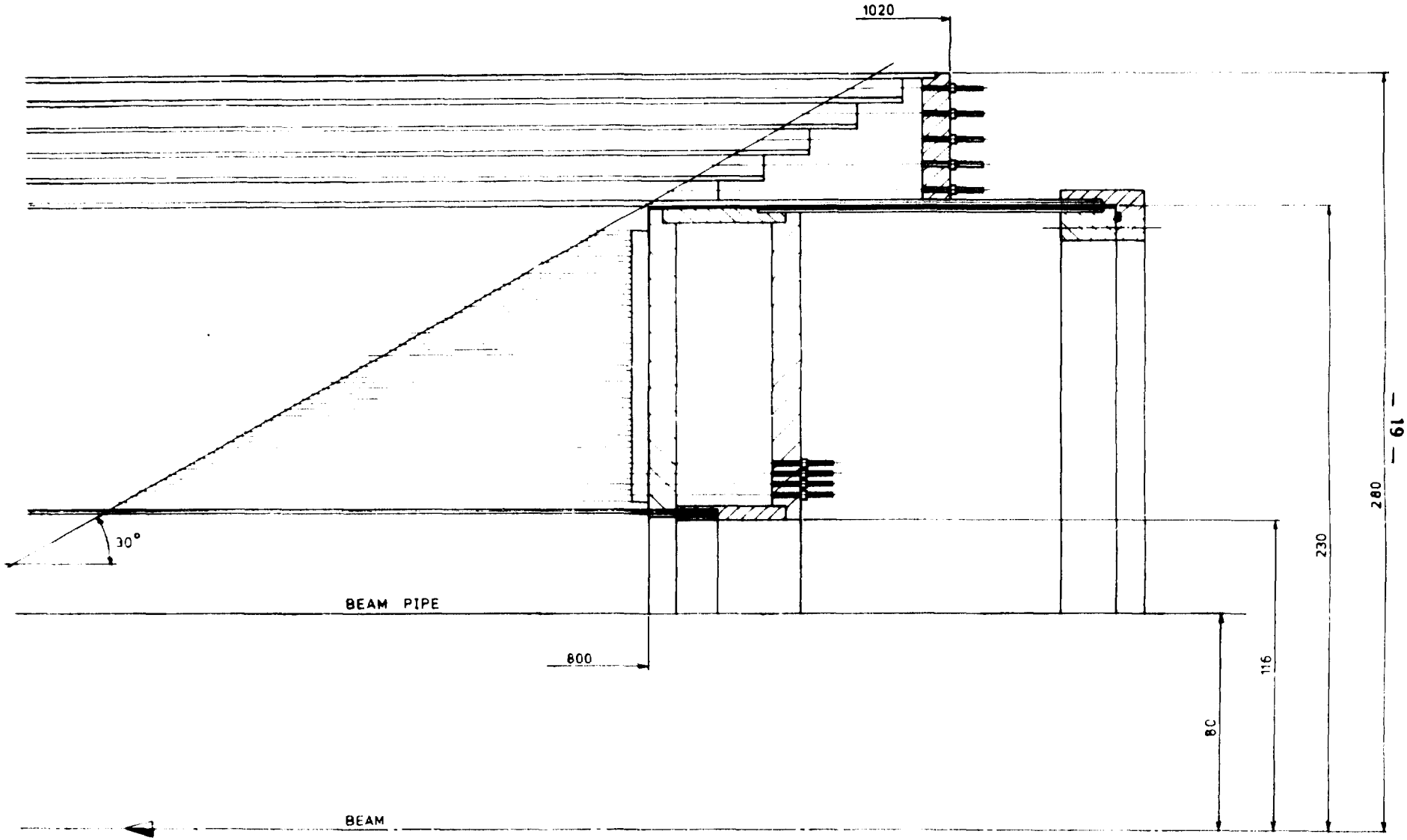

Fig. 2 LAYOUT INNERDETECTOR (revised feb 85)

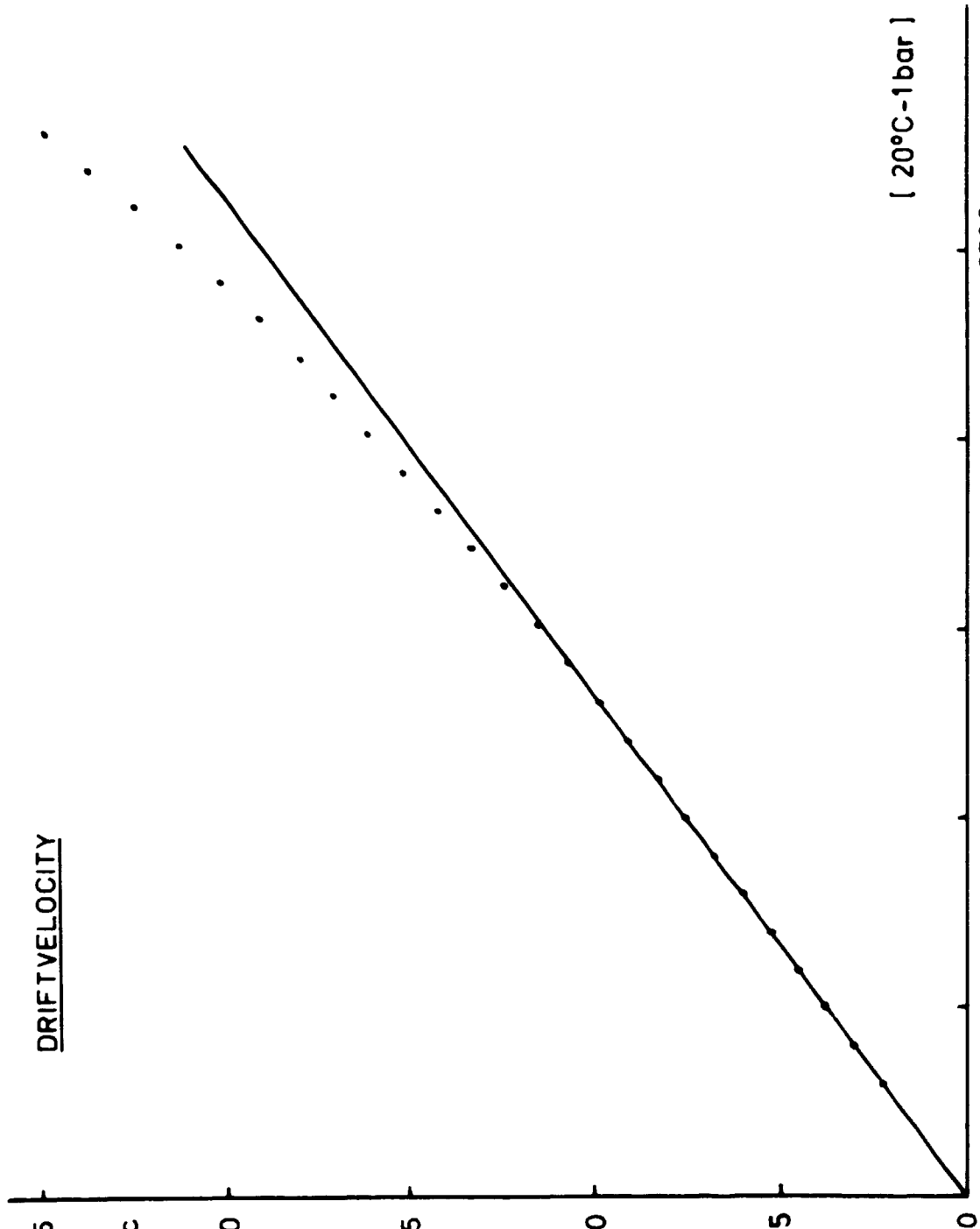
DRIFT VELOCITY
μm/nsec
25
20
15
10
5
0
500
1000
1500
2000
2500
E_D(V/cm)
[20°C-1bar]

Fig. 3

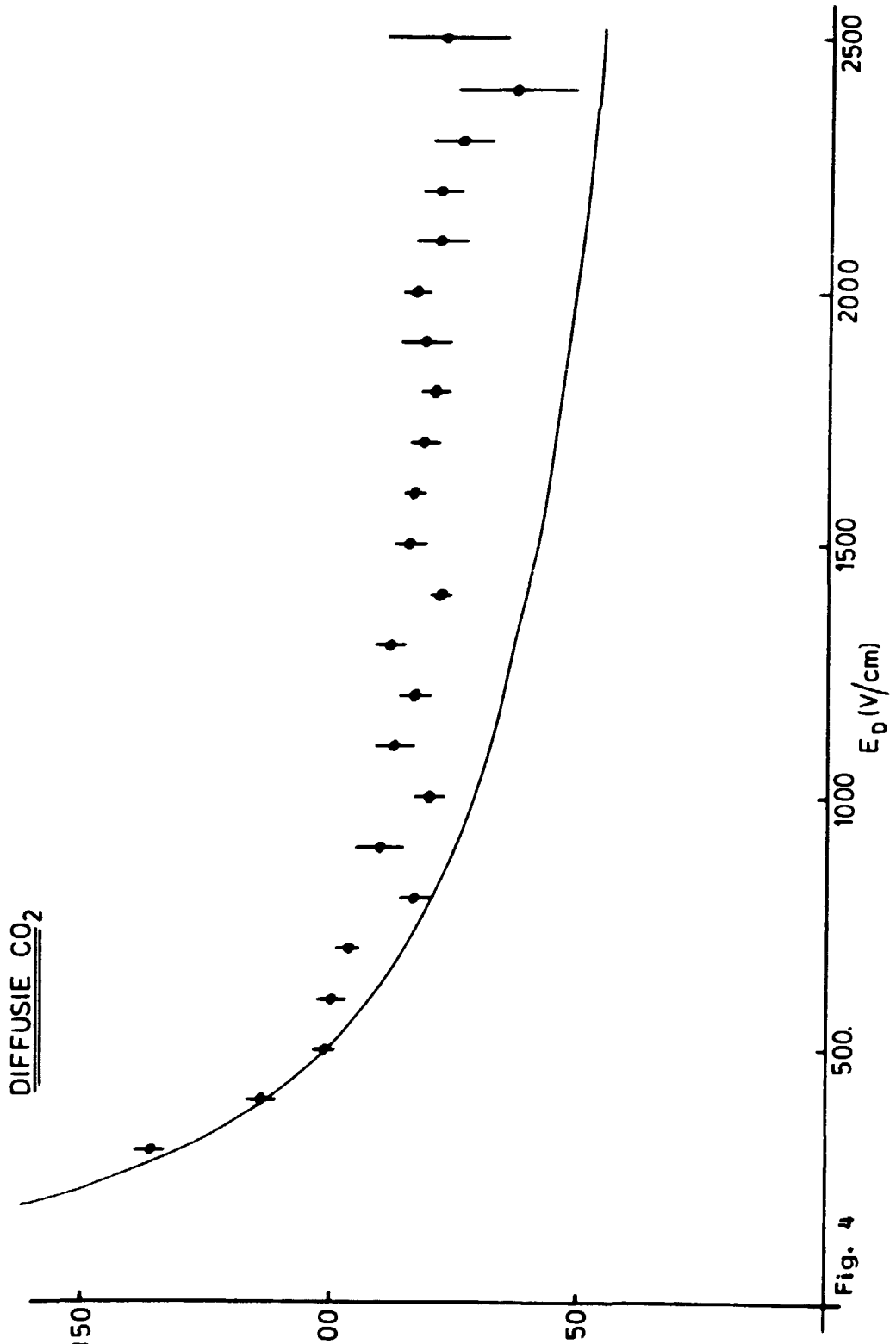
DIFFUSIE CO_2
D_l $\mu m/\sqrt{cm}$
150
100
50
500.
1000
1500
2000
2500
E_D (V/cm)

Fig. 4

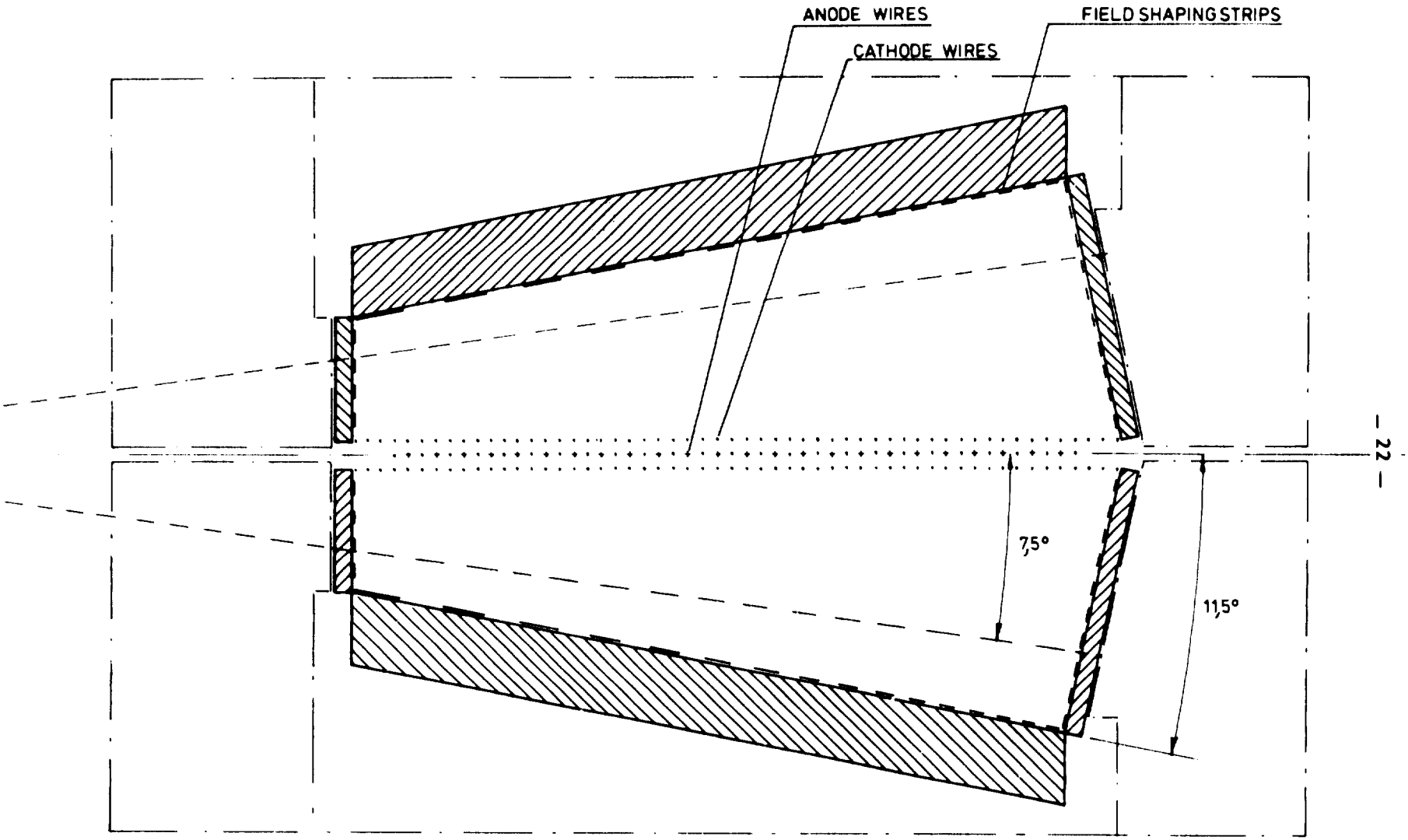

Fig. 5 JET TEST CHAMBER

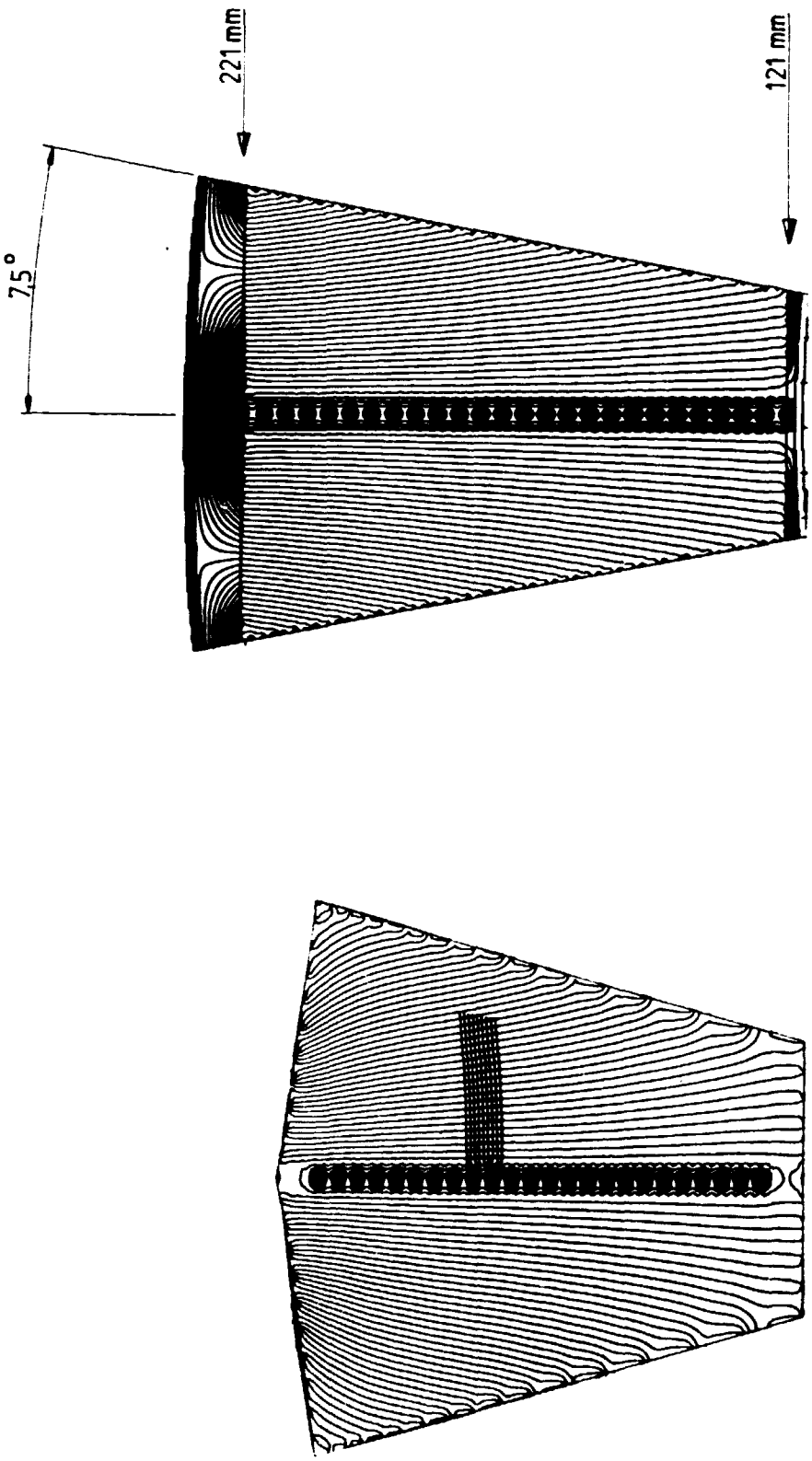

Fig. 6

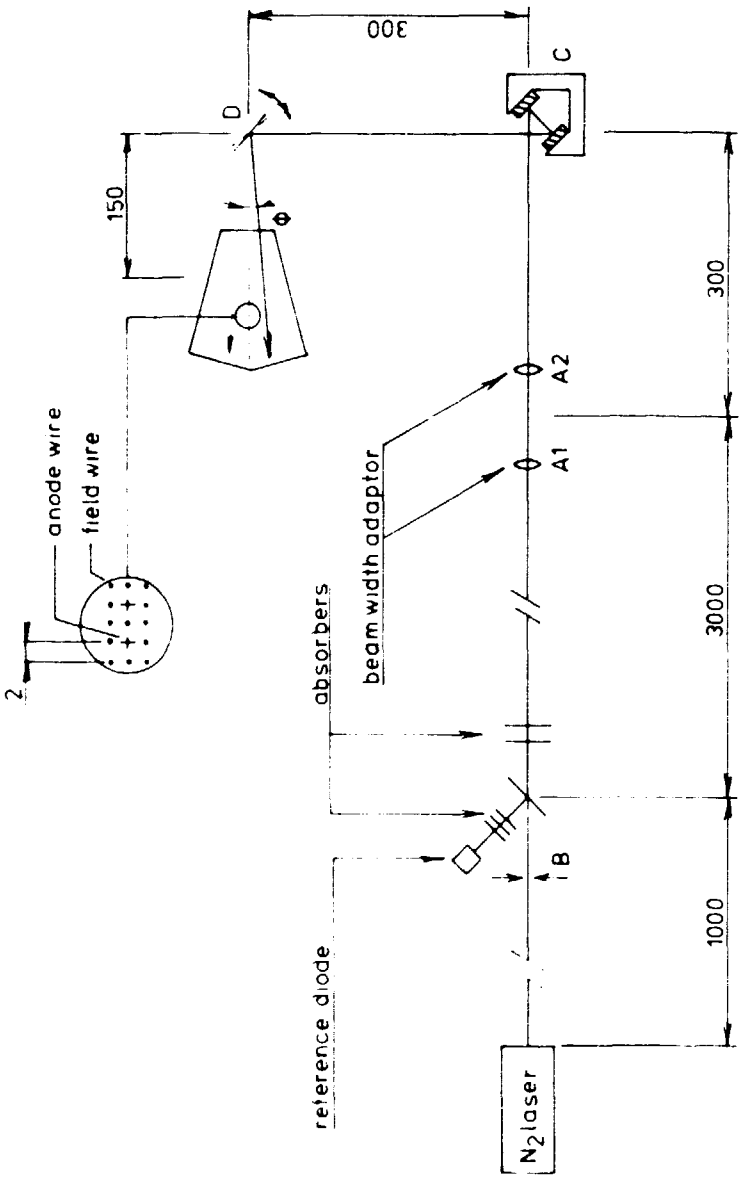

Fig. 7 TEST SETUP

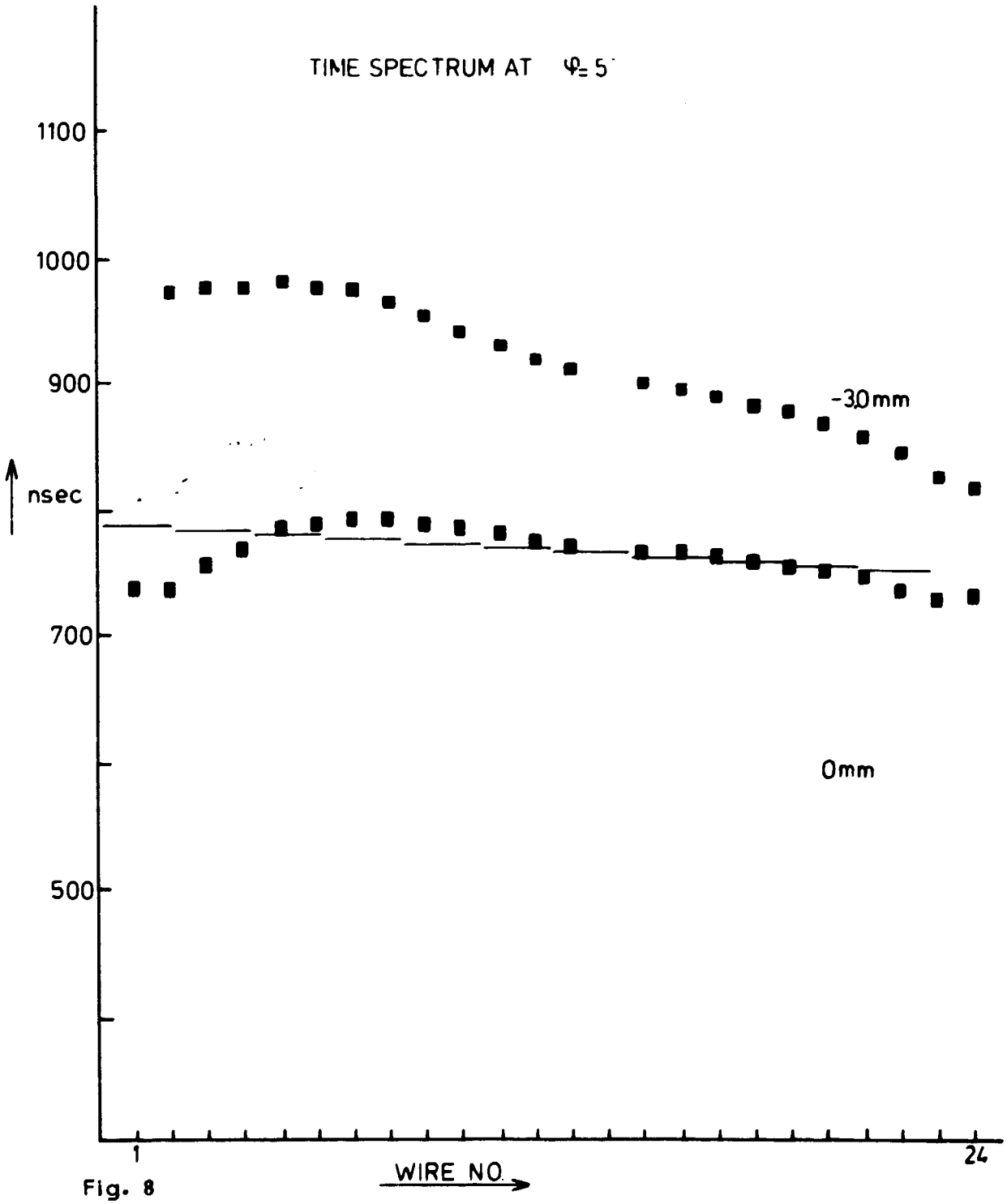
TIME SPECTRUM AT φ= 5°
1100
1000
900
700
500
nsec
-3.0mm
0mm
1
24
WIRE NO.

Fig. 8

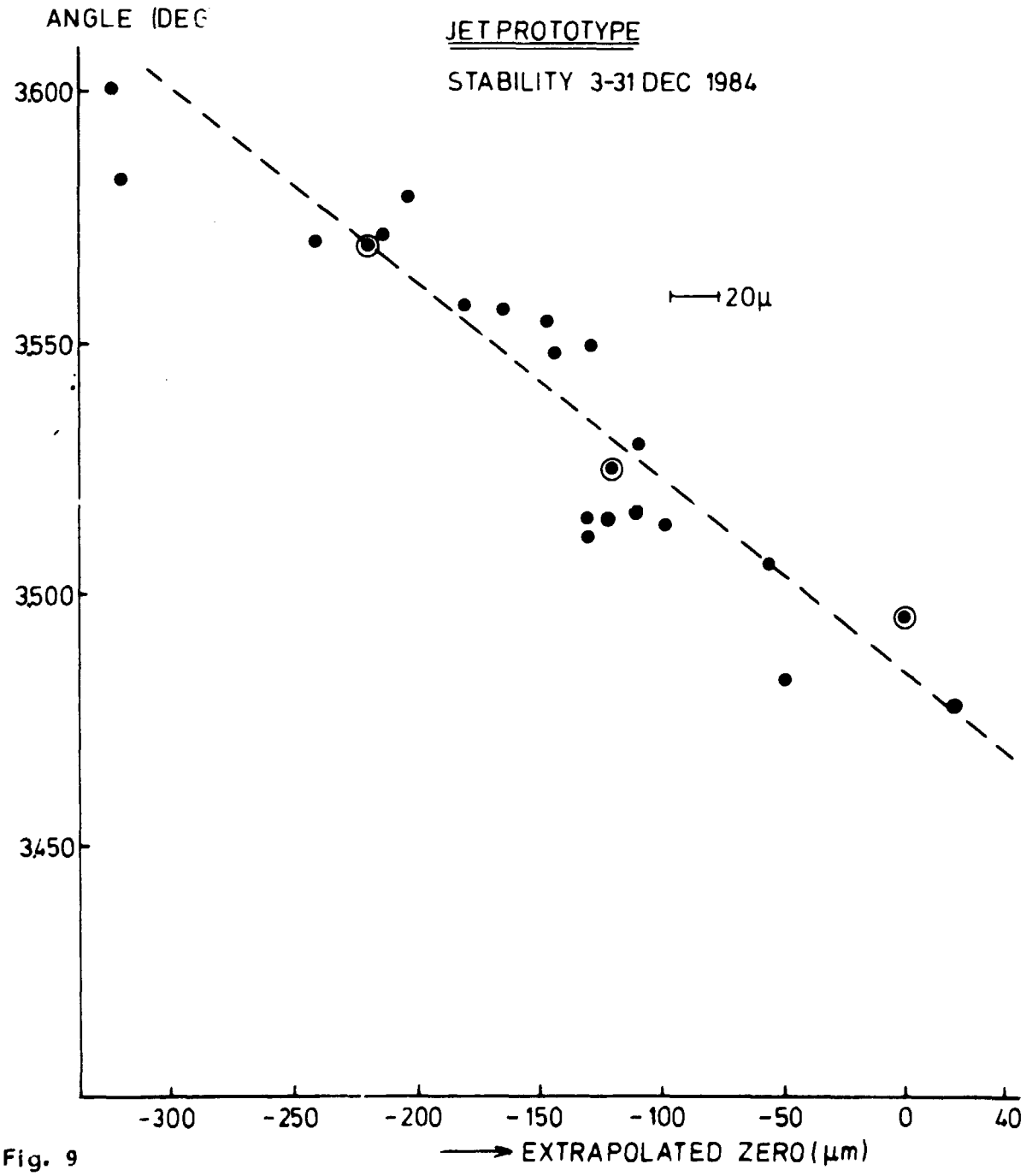
ANGLE (DEG
JET PROTOTYPE
STABILITY 3-31 DEC 1984
3600
3550
3500
3450
20μ
-300
-250
-200
-150
-100
-50
0
40
EXTRAPOLATED ZERO (μm)

Fig. 9

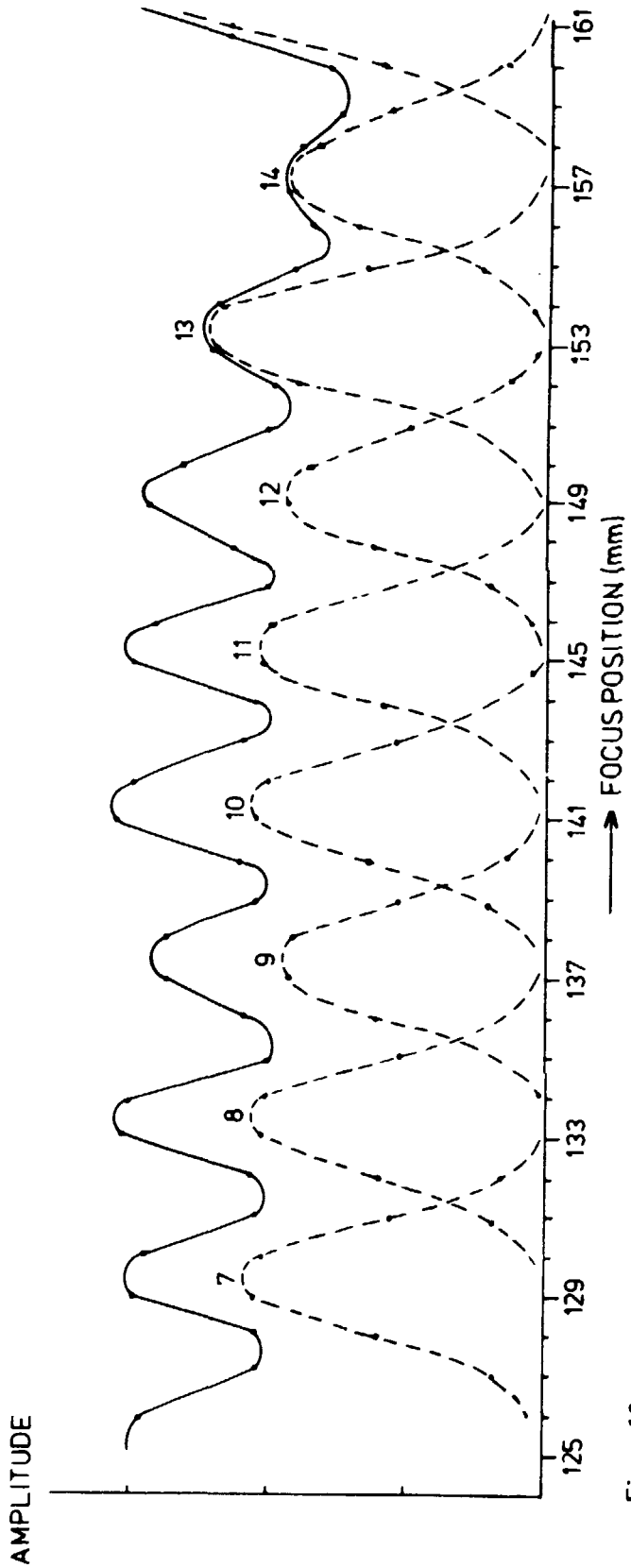
AMPLITUDE
7
8
9
10
11
12
13
14
125
129
133
137
141
145
149
153
157
161
FOCUS POSITION (mm)

Fig. 10

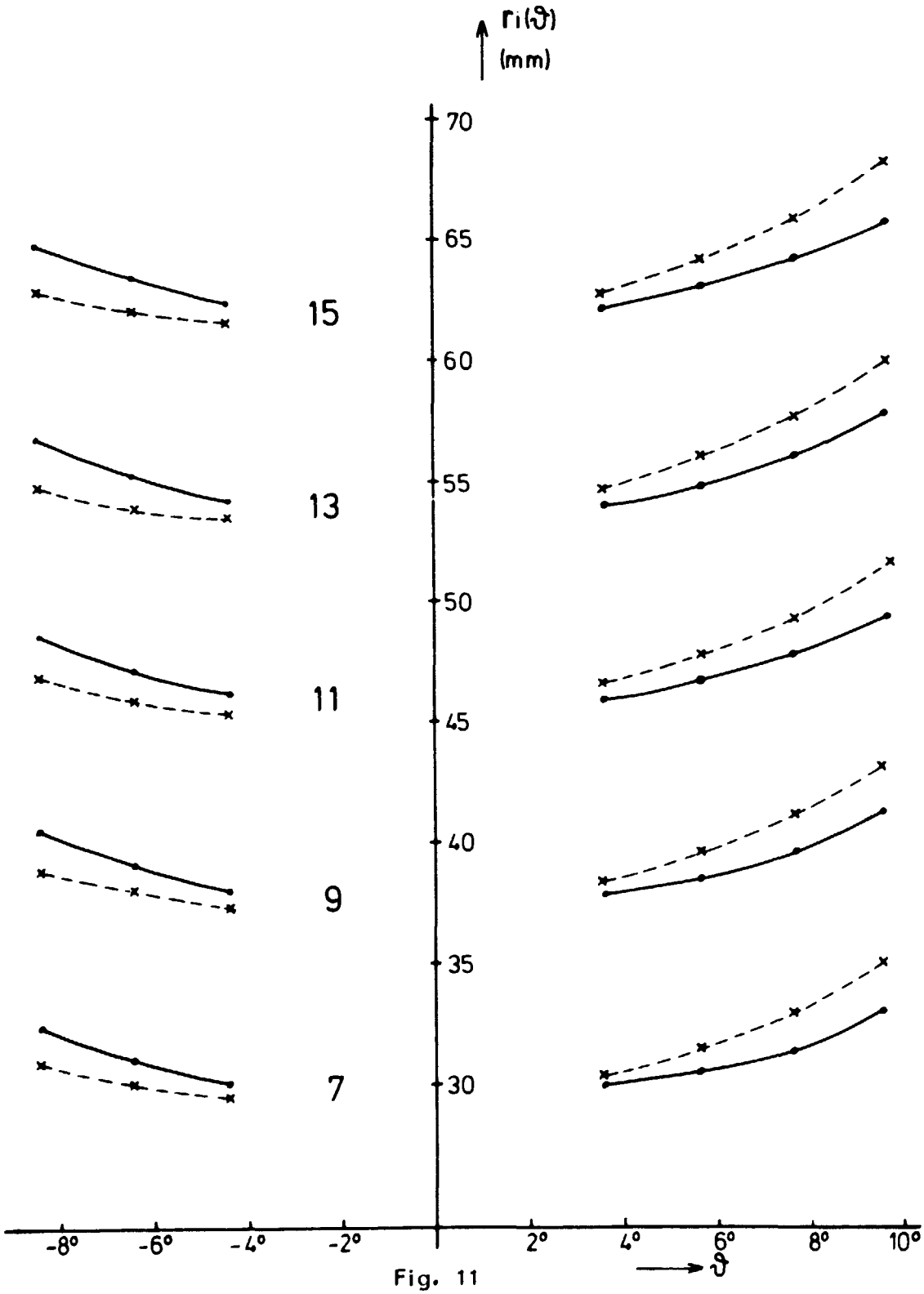

Fig. 11